Photochemical & Photobiological Sciences

PAPER

Titania hollow spheres modified with tungstophosphoric acid with enhanced visible light absorption for the photodegradation of 4-chlorophenol†

M. Á. Orellana,[a] L. Osiglio,[a] P. M. Arnal[b] and L. R. Pizzio*[a]

Received 31st May 2016,
Accepted 3rd October 2016

DOI: 10.1039/c6pp00175k

www.rsc.org/pps

Titania hollow spheres were synthesized using silica nanospheres as the template. The core was removed using NaOH solution. They were subsequently impregnated with tungstophosphoric acid (TPA) solutions and annealed at two different temperatures (100 and 500 °C). These materials were characterized by several physicochemical techniques (XRD, BET, SEM, DRS, FT-IR, FT-Raman and ^{31}P MAS-NMR). The ^{31}P MAS-NMR and FT-IR characterization showed that the main species present in the samples was the $[PW_{12}O_{40}]^{3-}$ anion, which was partially transformed into the $[P_2W_{21}O_{71}]^{6-}$ anion during the synthesis and drying step. ^{31}P MAS-NMR, and FT-Raman characterization revealed the evidence of a strong interaction between the Keggin anion of TPA and TiO_2 surfaces, possibly due to the formation of surface heteropolyacid-TiO_2 complexes. The DRS results showed that the absorption threshold onset continuously shifted to the visible region with increased TPA concentration and calcination at 500 °C. The enhanced visible light absorption could be related to the formation of a surface complex TPA Keggin anion–TiO_2. The catalytic activity of the materials in the photodegradation of 4-chlorophenol under UV and visible light irradiation increased when the TPA content and the calcination temperature of the samples were raised.

1. Introduction

The potential of heterogeneous photocatalysis over TiO_2 to destroy a wide range of waterborne pollutants and microorganisms has aroused enormous interest.[1,2] The preparation of titania-based photocatalysts with high catalytic performance has also attracted much attention. TiO_2 has been the most widely used because it is easily available, inexpensive, nontoxic, and it shows relatively high chemical stability.[3]

It is claimed that titania performance in the photodegradation of contaminants contained in wastes depends on its crystal structure, crystallinity, surface area, surface hydroxyl density, band gap energy, and morphology,[4] among other factors. The low surface area and the fast recombination of the photoinduced electrons and holes are the main effects that can lead to a low photocatalytic activity. Additionally, titania absorbs only UV light, which is not abundant on earth's surface, representing an enormous limitation in solar-driven photocatalytic processes.

In the last few years, the synthesis of titania hollow microspheres (@TiO_2) has attracted much attention due to their large surface area, low density, and highly efficient light-harvesting properties.[5–9]

They were successfully synthesized using pentahydrated copper sulfate,[6] latex[7] or silica[9,10] spheres as templates. The synthesis using a template free solvothermal method has been also performed.[8]

Additionally, shell and core–shell particles (@TiO_2 and SiO_2@TiO_2, respectively) may be less harmful to biological systems than TiO_2 nanoparticles.[10]

Tungstophosphoric and tungstosilicic acid (TPA and TSA, respectively) were employed as effective homogeneous photocatalysts in the degradation of organic pollutants in water. They have also been used to modify TiO_2 in order to reduce the charge recombination and enhance visible light absorption.[3]

The photocatalytic degradation of 4-chlorophenol (4-CP) has been investigated by many research groups and has become a standard reaction for evaluating various experimental parameters in photocatalysis.[11–13]

We present here, for the first time, the preparation and characterization of titania hollow microspheres modified with

[a]Centro de Investigación y Desarrollo en Ciencias Aplicadas "Dr. Jorge J. Ronco" (CINDECA), Facultad de Ciencias Exactas, UNLP-CCT La Plata, CONICET, 47 No 257, 1900-La Plata, Argentina. E-mail: lrpizzio@química.unlp.edu.ar
[b]CETMIC, Centro de Tecnología de Recursos Minerales y Cerámica, CIC-CONICET Gonnet, La Plata, Argentina

†Electronic supplementary information (ESI) available. See DOI: 10.1039/c6pp00175k

TPA. The influence of some preparation conditions on the catalytic activity in 4-CP photodegradation was studied.

2. Experimental section

2.1. Catalysts' synthesis

Nano-spherical particles with an amorphous, solid core of SiO_2 and a porous, polycrystalline shell of TiO_2 were formed in a three-step procedure.[10] The first step yielded silica spheres, the second step, silica spheres covered with a layer of amorphous titanium oxide (SiO_2@TiO_2), and in the last step titanium oxide crystallized in a shell after a mild acidic chemical treatment. Finally, the silica core was removed using a NaOH solution, yielding titania hollow spheres (@TiO_2). The modification @TiO_2 with tungstophosphoric acid ($H_3PW_{12}O_{40}$) was realized by wet impregnation. The amount of TPA in the solution was fixed in order to obtain TPA concentrations of 10, 20 and 30% by weight in the final material. The system was kept at room temperature until dry. The solids were thermally treated at 100, and 500 °C for 2 h, and were named @TiO_2TPAXX$_{T100}$ and @TiO_2TPAXX$_{T500}$, respectively, where XX was the TPA concentration. The TPA content in the @TiO_2TPAXX samples was estimated as the difference between the W amount contained in the tungstophosphoric acid water solution originally used for the impregnation and the amount of W that remained in the beaker after removing the dried samples. Finally, in order to remove the TPA weakly bound to the titania surface, the materials were brought into contact with water (typically 1 g in 1 l) for 24 h, filtered, and dried at 100 °C. The amount of W in the water solutions obtained after the ground solids were extracted was determined by atomic absorption spectrometry using a Varian AA Model 240 spectrophotometer. The calibration curve method was used with standards prepared in the laboratory. The analyses were carried out at a wavelength of 254.9 nm, bandwidth of 0.3 nm, lamp current of 15 mA, phototube amplification of 800 V, and burner height of 4 mm, and using acetylene–nitrous oxide flame (11 : 14).

2.2. Catalyst characterization

The specific surface area of the solids was determined from N_2 adsorption–desorption isotherms at liquid-nitrogen temperature. They were obtained using Micromeritics ASAP 2020 equipment. The samples were previously degassed at 100 °C for 2 h. Powder XRD patterns were obtained on Philips PW-1732 with a built-in recorder, using Cu Kα radiation, a nickel filter, 20 mA and 40 kV in the high voltage source, and a scanning angle between 5 and 60° of 2θ at a scanning rate of 1° per minute. FT-IR spectra of the supports and catalysts were obtained in the 400–4000 cm^{-1} wavenumber range using a Bruker IFS 66 FT-IR spectrometer and pellets in KBr. Fourier transform Raman spectra were recorded on a Raman Horiba Jobin-Yvon T 64 000 instrument with an Ar+ laser source of 488 nm wavelength in a macroscopic configuration. The ^{31}P MAS-NMR spectra were recorded using the CP/MAS ^{1}H–^{31}P technique with Bruker Avance II equipment. A sample holder of 4 mm diameter and 10 mm height was employed, using 5 μs pulses, and a repetition time of 4 s, working at a frequency of 121.496 MHz for ^{31}P at room temperature. The spin rate was 8 kHz and several hundred pulse responses were collected. Phosphoric acid 85% was employed as an external reference. DRS spectra of samples were recorded using a UV-visible Lambda 35, Perkin Elmer spectrophotometer, to which a diffuse reflectance chamber with an integrating sphere of 50 mm diameter and internal Spectralon coating is attached. The range covered was 200–800 nm. The secondary electron micrographs (SEM) and the energy dispersive X-ray (EDX) patterns of the samples were obtained using Phillips 505 Model scanning electron microscopy equipment and an EDAX 9100 analyser at a working potential of 15 kV and graphite-supported samples metallized with gold.

Transmission electron microscopy (TEM) was performed on a JEOL 100 CXII microscope, working at 100 kV and at a magnification of 80 000×. The samples were crushed in an agate mortar, ultrasonically dispersed in isobutanol, and deposited on a carbon-coated copper grid.

2.3. Catalytic test

The catalytic activity of the materials was evaluated in the photodegradation of 4-chlorophenol (4-CP) in water, at 25 °C. The tests were carried out employing 5 UV black light lamps Philips TLD 18 W (emission spectra: 330–400 nm and UV intensity between 300 and 400 nm: 38 W m^{-2}) or 5 blue fluorescent lamps Philips TLD-18 W (emission spectra: 400–500 nm with UV intensity: 0.1 W m^{-2} and global intensity between 290 and 1100 nm: 60 W m^{-2}). UV and global intensities were monitored with a Kipp & Zonen (CM3) power meter (Omni instruments Ltd, Dundee, UK). The catalyst was maintained in the suspension by stirring, and air was continuously bubbled. Previously, the 4-CP solution (100 ml, 1.5 10^{-4} mol l^{-1}) containing 50 mg of the catalyst was magnetically stirred in the absence of light for 60 min to ensure that the adsorption–desorption equilibrium of 4-CP on the surface of the materials is attained. The pH of the experiments was 6.9. During the course of the experiments, samples were periodically withdrawn, filtered using a Millipore syringe adapter (porosity, 0.45 μm) and then analyzed. The variation of the 4-CP concentration as a function of the reaction time was determined by using a UV-visible LAMBDA 35 Perkin Elmer double-beam spectrophotometer, measuring the absorbance at 225 nm. The concentration of the released chloride ions was measured by using a selective Cl^- electrode (pHoenix CLO1508) with an ion meter (Consort P903). The percentage of 4-CP mineralized was determined using the Total Organic Carbon, Method 10129 DR/4000 (HACH).

3. Results and discussion

According to the SEM micrograph (Fig. 1a), the silica cores (mean diameter in the range of 650–750 nm) present a smooth

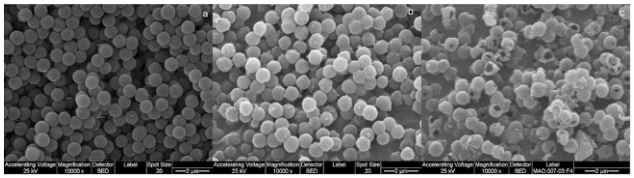

Fig. 1 SEM micrographs of SiO_2 (a), SiO_2@TiO_2 (b) and @TiO_2 (c).

surface and are well dispersed, without the formation of silica aggregates. On the other hand, the SiO_2@TiO_2 sample (Fig. 1b) displays a rough surface and diameters in the range of 800–900 nm.

For the @TiO_2 material (Fig. 1c), the thickness of the titania layer estimated by TEM is around 70 nm. No significant changes in the morphology of the samples after the impregnation with TPA and the thermal treatment were detected by SEM and TEM. Analyses performed by EDX show that the silica core was successfully removed using a NaOH solution. The EDX measurements (see the ESI†) revealed the presence of the Si Kα (at 1.74 keV) and Ti Kα (4.51 keV) signals in SiO_2@TiO_2 and @TiO_2 samples. For the SiO_2@TiO_2 material, the ratio between the Si Kα and the Ti Kα signal area (A_{Sik}/A_{Tik}) was 1.43. This value was significantly lower for the @TiO_2 sample (A_{Sik}/A_{Tik} = 0.22) due to the almost complete silica core elimination.

The N_2 adsorption–desorption isotherms of @TiO_2TPAXX$_{T100}$ and @TiO_2TPAXX$_{T500}$ samples can be classified as type IV, characteristic of mesoporous materials. For all the materials the hysteresis loop (H2 type) was very small.

The specific surface area (S_{BET}) of the @TiO_2TPAXX$_{T100}$ and @TiO_2TPAXX$_{T500}$ samples determined from N_2 adsorption–desorption isotherms using the Brunauer–Emmett–Teller (BET) method, together with the average pore diameter (D_p), are shown in Table 1. The specific surface area of the micropores (S_{micro}) was estimated by the *t*-plot method. As can be observed, all the samples are mesoporous materials with a D_p higher than 9.0 nm. The S_{BET} decreased and the mean pore radius increased when both the TPA content and the temperature of the thermal treatment were raised.

Taking into account the values of S_{micro}, less than 10% of the total surface area resulted from a microporous structure. The XRD pattern of @TiO_2 calcined at 100 °C exhibited only a wide peak at 2θ = 25.2° (101) assigned to the anatase phase. The XRD pattern of @TiO_2 treated at 500 °C also presents three new wide peaks at 37.9 (004), 47.8 (200) and 54.3° 2θ, due to the increment of the crystallinity (see the ESI†).

Table 1 Textural properties of @TiO_2TPAXX materials

	S_{BET} (m^2 g^{-1})		$D_{p\ BJH}$ (nm)	
Samples	T100	T500	T100	T500
@TiO_2	77	46	9.9	15.2
@TiO_2TPA10	65	26	10.1	18.9
@TiO_2TPA20	34	23	13.8	19.0
@TiO_2TPA30	16	13	19.1	21.3

On the other hand, for the @TiO_2TPA10$_{T100}$ sample, no diffraction lines attributed to crystalline TPA or its decomposition products were present in the XRD pattern. However, a new set of peaks ascribed to the $H_3PW_{12}O_{40}{\cdot}6H_2O$, (one of the more common tungstophosphoric acid hydrates) is present in the XRD pattern of the @TiO_2TPA20$_{T100}$ and @TiO_2TPA30$_{T100}$ samples.[14]

The patterns of the @TiO_2TPA10$_{T500}$, @TiO_2TPA20$_{T500}$ and @TiO_2TPA30$_{T500}$ samples only showed the characteristic peaks of the anatase phase; no diffraction lines corresponding to TPA were observed indicating that the species present are highly dispersed as a noncrystalline form or as crystallites low enough to be detected by this technique.

The leaching experiments revealed that TPA was firmly attached to the titania surface (less than 3% of the TPA content was eliminated). In the case of the @TiO_2TPA10$_{T100}$, @TiO_2TPA10$_{T500}$, and @TiO_2TPA20$_{T500}$ samples, the loss of TPA was practically negligible (0.90%, 0.50%, and 0.65% respectively). For all the TPA contents, the loss was lower when the samples were treated at 500 °C (for example, 2.90% and 1.75% for @TiO_2TPA30$_{T100}$ and @TiO_2TPA30$_{500}$, respectively).

It is worthy of mention that the peaks in the XRD patterns of the @TiO_2TPA20$_{T100}$ and @TiO_2TPA30$_{T100}$ samples assigned to the $H_3PW_{12}O_{40}{\cdot}6H_2O$ disappear as a result of leaching. We can suggest that the loosely bound TPA eliminated during the leaching experiments was mainly the $H_3PW_{12}O_{40}{\cdot}6H_2O$ hexahydrate. In this case, a hydrogen bond type interaction between oxygen atoms [W=O and W–O–W] of TPA species and hydroxyl groups [Ti–OH] of the titania matrix could take place.

However, when TPA is firmly attached to the titania surface the interaction can be of the electrostatic type due to transfer of protons to Ti–OH according to:[15]

$$\text{Ti–OH} + H_3PW_{12}O_{40} \rightarrow [\text{Ti–OH}_2^{+}]\ [H_2PW_{12}O_{40}^{-}].$$

Taking into account Lefebvre's report,[16] we can assume that the elimination of water from [Ti–OH_2^+] during the thermal treatment should involve direct bonding of the polyanion to titania [Ti–O–W].

Li *et al.* have suggested that TPA could interact with titania surfaces through Ti–O–W covalent bonds formed by the interaction of W=O or W–O–W bonds with Ti–OH species.[17,18]

^{31}P MAS-NMR spectra corresponding to the @TiO_2TPAXX$_{T100}$ (Fig. 2) and @TiO_2TPAXX$_{T500}$ materials show two signals; the more intense at −14.2 ppm attributed to the $[PW_{12}O_{40}]^{3-}$ anion and the other at −12.4 ppm, to the dimer $[P_2W_{21}O_{71}]^{6-}$.[19] The transformation of the $[PW_{12}O_{40}]^{3-}$ anion into the dimer is due to the limited stability range of the Keggin anion in solution. At pH 1.5–2, it is reversibly and quickly transformed according to the scheme: $[PW_{12}O_{40}]^{3-} \Leftrightarrow [P_2W_{21}O_{71}]^{6-} \Leftrightarrow [PW_{11}O_{39}]^{7-}$ when the hydroxyl concentration is increased.[20]

The downfield shift and slight increase of the line width observed, compared to the bulk compound (−15.3 ppm), can

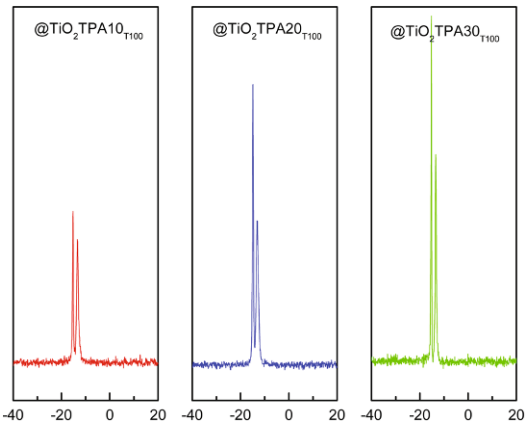

Fig. 2 ^{31}P MAS-NMR spectra of @TiO_2TPAXX$_{T100}$ samples.

be attributed to the interaction between the anion and the titania matrix[21] such as $[{=}Ti{-}OH_2^+][H_{3-X}PW_{12}O_{40}]^{X-}$.

The ^{31}P MAS-NMR spectra of the @TiO_2TPAXX$_{T500}$ samples show that the ratio between the intensity of the signal attributed to the $[PW_{12}O_{40}]^{3-}$ Keggin anion and the one assigned to the dimer $[P_2W_{21}O_{71}]^{6-}$ increases with the increment of the calcination temperature. We have reported[3] that a noticeable transformation of the $[PW_{12}O_{40}]^{3-}$ anion into the dimeric one takes place when the thermal treatment is performed at temperatures higher than 400 °C. Nevertheless, the line assigned to the $[PW_{12}O_{40}]^{3-}$ anion is the most intense in all the samples. Additionally, the calcination at 500 °C produces a slight increment of the line at −14.2 ppm that could be related with the direct bonding of the polyanion to titania [Ti–O–W].

The FT-IR spectrum of TPA (Fig. 3) shows bands at 1081, 982, 888, 793, 595, and 524 cm^{-1}, in agreement with those reported in the literature for the $H_3PW_{12}O_{40}$ acid.[22] They are assigned to the stretching vibrations P–Oa, W–Od, W–Ob–W, and W–Oc–W, and to the bending vibration Oa–P–Oa, respectively. In the FT-IR spectra of the @TiO_2TPAXX$_{T100}$ samples,

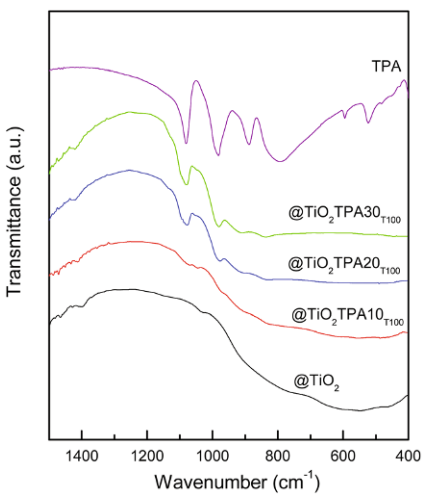

Fig. 3 FT-IR spectra of @TiO_2, TPA, and @TiO_2TPAXX$_{T100}$ samples.

the P–O_a, W–O_d, and W–O_b–W stretching vibrations of the $[PW_{12}O_{40}]^{3-}$ anion are overlapped to the TiO_2 wide band. The main FT-IR bands assigned to the stretching vibrations P–Oa (1095 and 1085 cm^{-1}), W–Od (972 cm^{-1}), and W–O–W (890 and 790 cm^{-1}) of the dimer $[P_2W_{21}O_{71}]^{6-}$ appear at wavenumber values similar to those of the $[PW_{12}O_{40}]^{3-}$ Keggin anion.[23] For the @TiO_2TPA20$_{T100}$ and @TiO_2TPA30$_{T100}$ samples the band at 1080 cm^{-1} displays a shoulder (at 1094 cm^{-1}) assignable to the presence of the $[P_2W_{21}O_{71}]^{6-}$ anion.

From the FT-IR and ^{31}P MAS-NMR results, we can state that the main species present in the samples is the $[PW_{12}O_{40}]^{3-}$ Keggin anion. However, it was partially transformed into the $[P_2W_{21}O_{71}]^{6-}$ dimer during the synthesis and drying steps.

The main Raman vibration bands of bulk TPA appear at 1010, 990 and 930 cm^{-1}.[24] They present an important broadening when TPA is supported on @TiO_2. Additionally, in the spectra of the @TiO_2TPAXX$_{T500}$ samples, the main Raman scattering peak of TiO_2 at 141 cm^{-1} exhibits a strong blue shift and broadening. In agreement with Li *et al.*[25] we consider that the shift and broadening of the Raman vibration modes of TPA and TiO_2 could be associated with a strong interaction between the TiO_2 network and TPA.

The UV-vis-DRS spectrum of bulk TPA presented two absorption bands in the range of 200–450 nm, assigned to the charge transfer from bridging or terminal O 2p to W 5d (W–O–W and W–Od, respectively).[3] On the other hand, the @TiO_2 sample displayed intense absorption in the range of 200–390 nm, corresponding to charge transfer from the valence band (O 2p) to the conduction band (Ti 3d).[26]

The UV-vis-DRS spectra of the @TiO_2TPAXX$_{T100}$ and @TiO_2TPAXX$_{T500}$ samples (Fig. 4a and b respectively) show an absorption threshold onset that continuously shifts to the visible region with the increment of the TPA content. The DRS results also reveal that the visible light absorption increases when the calcination temperature is raised up to 500 °C. So, the TPA–TiO_2 surface complex could be responsible for the visible light absorption and spectroscopic changes observed.

We evaluated the activity of the synthesized materials in the photocatalytic degradation of 4-chlorophenol at the pH of the suspension obtained by addition of the catalyst to 4-CP water solution. The initial and the final pH of the solutions were in the range of 6.9–5.7.

The point of zero charge (pH_{PZC}) of the @TiO_2TPAXX$_{T100}$ samples (estimated using the mass titration method proposed by Noh and Schwarz[27]) decreases in the following order: @TiO_2TPA10$_{T100}$ (5.4) > @TiO_2TPA20$_{T100}$ (4.9) > @TiO_2TPA30$_{T100}$ (4.3) due to the incorporation of TPA. In the case of the samples treated at 500 °C, the behaviour is the same: @TiO_2TPA10$_{T500}$ (5.2) > @TiO_2TPA20$_{T500}$ (4.1) > @TiO_2TPA30$_{T500}$ (2.7). However, the values are slightly lower than those of the @TiO_2TPAXX$_{T100}$ samples due to the elimination of water from $[Ti{-}OH_2^+]$ during the thermal treatment. So, under our experimental conditions, the surface of the @TiO_2TPAXX samples was mostly negatively charged. As a result, 4-CP is not significantly adsorbed on the catalyst surface.

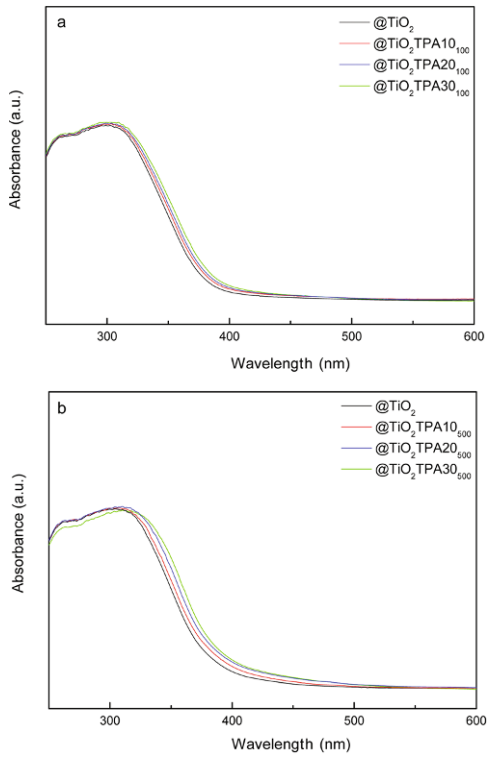

Fig. 4 DRS spectra of @TiO_2, and @TiO_2TPAXX samples calcined at 100 (a) and 500 °C (b).

Experiments made without the catalyst (under UV-A and visible irradiation), showed negligible 4-CP degradation after 240 min of irradiation.

The variation of the 4-CP concentration as a function of time using the @TiO_2TPAXX$_{T100}$ and @TiO_2TPAXX$_{T500}$ catalysts is shown in Fig. 5.

The reduction in the 4-CP concentration was rather low (31%) for the titania hollow spheres treated at 100 °C after 240 min of irradiation. However, 4-CP degradation significantly increases in parallel with the increment of tungstophosphoric acid: @TiO_2TPA10$_{T100}$ (69%) < @TiO_2TPA20$_{T100}$ (85%) < @TiO_2TPA30$_{T100}$ (92%). This behavior is due to the fact that TPA on the TiO_2 surface acts as an effective trap of photoinduced electrons. Electrons can be easily transferred from the TiO_2 conduction band to TPA Keggin anions on the surface, decreasing the fast e^-/h^+ recombination[28] and leaving more valence band holes (h^+VB) available to react with water molecules to yield $^{\bullet}$OH radicals.

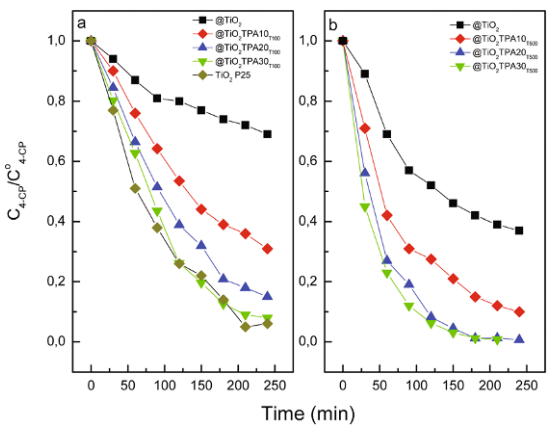

Fig. 5 Photocatalytic degradation of 4-CP as a function of the time (under UV-A irradiation) for @TiO_2, and @TiO_2TPAXX samples treated at 100 °C (a), 500 °C (b), and TiO_2 Evonik P25.

Additionally, the increment of the catalytic activity could be due to the direct participation of TPA in the degradation of the organic substrate.[3] TPA absorb strongly in the UV region of the light spectrum (λ < 400 nm). This absorption corresponds to the ligand-to-metal charge-transfer band and it can generate strongly oxidizing excited state TPA*. They can perform the oxidation of organic substrates directly *via* charge transfer or indirectly through the production of $^{\bullet}$OH reactive species that participates in the degradation of the organic substrate.[29,30] After that, the corresponding reduced TPA^- are usually re-oxidized to their original oxidation state by an electron acceptor such as dioxygen.

The degradation profile of 4-CP using TiO_2 Evonik P25 (commonly used as reference) was very similar to that of the @TiO_2TPA30$_{T100}$ sample.

Fig. 5b shows that the 4-CP amount degraded after 240 min of UV irradiation increased when the calcination temperature was raised up to 500 °C. For any TPA content considered, we observed that the 4-CP degraded amount increases with the increment of the calcination temperature (*i.e.*, @TiO_2TPA10$_{T500}$ (90%) > @TiO_2TPA10$_{T100}$ (69%)). This can be due to an increase in the crystallinity of the @TiO_2, resulting in a decrease in the number of defects that act as recombination centers for photogenerated electrons and holes.

For the @TiO_2TPAXX$_{T100}$ and @TiO_2TPAXX$_{T500}$ samples, we observed that the ratio between the amount of degraded 4-CP and the amount of released chloride ions as a function of the irradiation time remained practically equal to 1 during the course of the degradation. These results are in accordance with literature reports that evidence that the first step during the photocatalytic degradation of 4-CP is the Cl–aryl bond cleavage.

On the other hand, we found that the 4-CP amount degraded under blue-light irradiation (at 240 min), using titania hollow spheres modified with TPA as the catalyst, varied in the following way: @TiO_2TPA10$_{T500}$ (20%) < @TiO_2TPA20$_{T500}$ (27%) ≅ @TiO_2TPA30$_{T500}$ (29%). On the contrary, the catalytic activities of Evonik P25 and @TiO_2 were negligible. These results show the beneficial effect of TPA on the photocatalytic activity also under visible light radiation.

Under visible light irradiation the TPA anchored to the titania surfaces through Ti–O–W covalent bonds (responsible for the visible light absorption) would be excited yielding a TPA*–TiO_2 complex. The TPA*–TiO_2 complex can inject a photoexcited electron to TiO_2 CB.[31–33] Electron injection from TPA in the excited state (TPA*) to the CB of TiO_2 was clearly

observed using the two-color two-laser flash-photolysis technique.[33]

The electron injected to TiO_2 CB can react with molecular oxygen yielding a $^{\bullet}O_2^-$ radical. It is well known that in aqueous media this radical can undergo disproportion reactions producing mainly hydrogen peroxide.[34] H_2O_2 can also be reduced by CB electrons producing $^{\bullet}OH$ radicals that are also able to oxidize organic pollutants.

Nevertheless, the generation of hydrogen peroxide by means of disproportion of $^{\bullet}O_2^-$ radicals is very low in irradiated TiO_2 surfaces,[35,36] which should account for the low degradation of 4-CP.

It is worthy of mention that the @TiO_2TPA samples can be easily separated from the resulting suspension by decantation. On the contrary, Evonik P25 can be recovered only by filtration using Millipore filters. Taking into account the obtained results, @TiO_2TPA30_{T500} was chosen to test its reusability. To this end, after each photocatalytic experiment, the catalyst was easily separated from the resulting suspension by decantation, washed with distilled water, dried at 70 °C and reused four times (under UV-A irradiation).

The percentage of 4-CP degraded decreased slightly during the first and the second reuse (95% and 91% respectively), and then kept constant. The decrease could be assigned to the TPA solubilization (less than 1% of the TPA content), as was established by atomic absorption spectrometry. On the other hand, the mineralization degree was slightly lower than the amount of degraded 4-CP (78% and 70% for the first and the second reuse respectively) as a result of the formation of organic intermediates such as benzoquinone and hydroquinone.[37]

The activity of the @TiO_2TPA solids in the degradation of 4-chlorophenol aqueous solutions under UV and visible light irradiation increases with the TPA content and the thermal treatment temperature. The sample containing 30% TPA and annealed at 500 °C showed the highest photocatalytic activity. Furthermore, the reused catalysts showed only a slight decrease in the degradation and mineralization degree, thus being promissory materials to aid in the photocatalytic treatment of wastewater containing chlorinated phenols.

4. Conclusions

Titania hollow spheres were synthesized by the sol–gel method using silica nanospheres as the template. The direct modification of @TiO_2 with tungstophosphoric acid enables obtaining visible-light-absorbing materials. This fact could be due to the generation of surface complexes between TPA anions and TiO_2 through the formation of Ti–O–W bonds. Due to the formation of these bonds the main Raman scattering of TPA and TiO_2 displayed a strong blue shift and broadening.

The FT-IR and ^{31}P MAS-NMR results indicated that the main species present in the samples was the $[PW_{12}O_{40}]^{3-}$ anion, which was partially, transformed into the $[P_2W_{21}O_{71}]^{6-}$ dimeric anion during the synthesis and thermal treatment steps.

@TiO_2TPA materials exhibit higher photocatalytic activity than @TiO_2 under UV-A irradiation, since the TPA acts as a sink of conduction band photo-induced electrons decreasing the e^-/h^+ recombination leaving available more valence band holes to either directly oxidize malachite green molecules or produce $^{\bullet}OH$ radicals.

The visible light photocatalytic activity of these materials in the 4-CP degradation could be explained by the fact that the TPA–TiO_2 complex may be excited by visible light absorption and injection of an electron into the TiO_2 conduction band, inducing the indirect formation of $^{\bullet}OH$ radicals.

Finally, the direct modification of @TiO_2 with TPA is a good method to obtain catalysts with photocatalytic activity in the 4-chlorophenol degradation under UV-A and visible light irradiation.

Acknowledgements

Authors thank the financial support from CONICET (PIP 628) and Universidad Nacional de La Plata (UNLP) (Project number X638) and the technical assistance of M. Theiller (SEM/EDX analysis) and P. Fetsis (BET).

References

1 M. R. Hoffmann, S. T. Martin, W. Choi and D. W. Bahnemann, *Chem. Rev.*, 1995, **95**, 69–96.
2 T. Ochiai and A. Fujishima, *J. Photochem. Photobiol., C*, 2012, **13**, 247–262.
3 M. N. Blanco and L. R. Pizzio, *Appl. Catal., A*, 2011, **405**, 69–78.
4 K. B. Kyoko, S. Kazuhiro, K. Hitoshi, O. Kiyomi and A. Hironori, *Appl. Catal., A*, 1997, **165**, 391–409.
5 J. G. Yu, W. Liu and H. G. Yu, *Cryst. Growth Des.*, 2008, **8**, 930.
6 C. Jia, Y. Cao and P. Yang, *Funct. Mater. Lett.*, 2013, **6**, 1350025–1350026.
7 C. Liu, H. Yin, L. Shi, A. Wang, Y. Feng, L. Shen, Z. Wu, G. Wu and T. Jiang, *J. Nanosci. Nanotechnol.*, 2014, **14**, 7072–7078.
8 L. Yan, X. He, Y. Wang, J. Li and D. Wang, *J. Mater. Sci.: Mater. Electron.*, 2016, **27**, 4068–4073.
9 L. Li, S. Bai, W. Yin, S. Li, Y. Zhang and Z. Li, *Int. J. Hydrogen Energy*, 2016, **41**, 1627–1634.
10 A. L. Di Virgilio, I. Maisuls, F. Kleitz and P. M. Arnal, *J. Colloid Interface Sci.*, 2013, **394**, 147–156.
11 C. Castañeda, F. Tzompantzi, R. Gómez and H. Rojas, *J. Chem. Technol. Biotechnol.*, 2016, **91**, 2170–2178.
12 M. Wang, G. Fang, P. Liu, D. Zhou, C. Ma, D. Zhang and J. Zhan, *Appl. Catal., B*, 2016, **188**, 113–122.
13 Y. Yao, L. Jiao, N. Yu, J. Zhu and X. Chen, *Russ. J. Electrochem.*, 2016, **52**, 348–354.

14 J. B. Mioc, R. Z. Dimitrijevi, M. Davidovic, Z. P. Nedic, M. M. Mitrovic and P. H. Colomban, *J. Mater. Sci.*, 1994, **29**, 3705–3718.
15 V. M. Fuchs, E. L. Soto, M. N. Blanco and L. R. Pizzio, *J. Colloid Interface Sci.*, 2008, **327**, 403–411.
16 F. Lefebvre, *J. Chem. Soc., Chem. Commun.*, 1992, **10**, 756–757.
17 K. Li, Y. Guo, F. Ma, H. Li, L. Chen and Y. Guo, *Catal. Commun.*, 2010, **11**, 839–843.
18 K. Li, X. Yang, Y. Guo, F. Ma, H. Li, L. Chen and Y. Guo, *Appl. Catal., B*, 2010, **99**, 364–375.
19 M. T. Pope, *Heteropoly and Isopolyoxometalates*, Springer-Verlag, Heidelberg, 1983, p. 58.
20 R. Massart, R. Contant, J. Fruchart, J. Ciabrini and M. Fournier, *Inorg. Chem.*, 1977, **16**, 2916.
21 V. M. Mastikhin, S. M. Kulikov, A. V. Nosov, I. V. Kozhevnikov, I. L. Mudrakovsky and M. N. Timofeeva, *J. Mol. Catal. A: Chem.*, 1990, **60**, 65–70.
22 C. Rocchiccioli-Deltcheff, R. Thouvenot and R. Franck, *Spectrochim. Acta, Part A*, 1976, **32**, 587–597.
23 R. Contant, *Can. J. Chem.*, 1978, **65**, 568–573.
24 I. Holclajtner-Antunovic, D. Bajuk-Bogdanovic, A. Popa and S. Uskokovic-Markovic, *Inorg. Chim. Acta*, 2012, **383**, 26–32.
25 J. Li, W. Kang, X. Yang, X. Yu, L. Xu, Y. Guo, H. Fang and S. Zhang, *Desalination*, 2010, **255**, 107–116.
26 J. T. Yates, *Surf. Sci.*, 2009, **603**, 1605–1612.
27 J. S. Noh and J. A. Schwarz, *J. Colloid Interface Sci.*, 1988, **130**, 157–164.
28 H. Park and W. Choi, *J. Phys. Chem. B*, 2003, **107**, 3885.
29 R. R. Ozer and J. L. Ferry, *J. Phys. Chem. B*, 2000, **104**, 9444.
30 S. Antonaraki, T. M. Triantis, E. Papaconstantinou and A. Hiskia, *Catal. Today*, 2010, **151**, 119–124.
31 R. Sivakumar, J. Thomas and M. Yoon, *J. Photochem. Photobiol., C*, 2012, **13**, 277–298.
32 J. A. Rengifo-Herrera, M. N. Blanco and L. R. Pizzio, *Mater. Res. Bull.*, 2014, **49**, 618–624.
33 T. Tachikawa, S. Tojo, M. Fujitsutka and T. Majima, *Chem. – Eur. J.*, 2006, **12**, 3124–3131.
34 D. T. Sawyer and J. S. Valentine, *Chem. Res.*, 1981, **14**, 393–400.
35 Y. Nosaka, Y. Yamashita and H. Fukuyama, *J. Phys. Chem. B*, 1997, **101**, 5822–5827.
36 H. Sakai, R. Baba, K. Hashimoto, A. Fujishima and A. Heller, *J. Phys. Chem. B*, 1995, **99**, 11896–11900.
37 A. Mylonas and E. Papaconstantinou, *J. Photochem. Photobiol., A*, 1996, **94**, 77–82.

